

# Co-valorization of marine sediments and construction & demolition wastes through alkali activation



Kostas Komnitsas

School of Mineral Resources Engineering, Technical University Crete, Chania, Crete 73100, Greece

## ARTICLE INFO

### Article history:

Received 5 September 2016

Received in revised form 27 October 2016

Accepted 1 November 2016

Available online 2 November 2016

### Keywords:

Marine sediments

Construction & demolition wastes

Alkali activation

Compressive strength

## ABSTRACT

In the present experimental study, the co-valorization potential of marine sediments and construction & demolition wastes (C&D wastes) through alkali activation is investigated. Specimens were produced by mixing raw materials, namely marine sediments and C&D waste components (tiles, bricks and concrete) with the activating solution consisting of KOH and sodium silicate solution. The produced specimens were then subjected to compressive strength testing. The effect of the molarity of the alkaline activating solution as well as the percentage of each waste in the initial mixture on the compressive strength of the final products was also assessed. Also, the effect of high temperature heating (400–800 °C), immersion in water or seawater and subjection to freeze–thaw cycles on the structural integrity of the produced specimens was investigated. Analytical techniques, namely X-ray Diffraction (XRD), Fourier Transform Infrared Spectroscopy (FTIR) and Scanning Electron Microscopy (SEM) were used for the identification of the morphology and structure of the final products.

© 2016 Elsevier Ltd. All rights reserved.

## 1. Introduction

Alkali activation of aluminosilicates can be accomplished at relatively low temperature and results in the production of materials, called geopolymers or inorganic polymers [1]. These cementitious materials, consisting of Si–O–Al bonds, are characterized by partially or fully amorphous polymeric structure, high early strength and high chemical and temperature resistance. They are suitable for a number of applications in the construction industry and are characterized by lower environmental footprint when compared with traditional construction materials, such as Ordinary Portland Cement (OPC) and concrete [2–5]. Although geopolymers can be produced with cost and properties comparable to OPC, there are some drawbacks such as loss of workability, quick setting time as well as health and safety implications when working with strong alkali solutions. This is the main reason why geopolymers have been proposed to be used mainly as pre-cast concrete (in railway traverses, pipelines, hydraulic structures, pre-tensioned concrete structures etc), where the above drawbacks can be easily adapted.

Today, most research efforts focus on valorization of several solid waste streams and the production of materials with suitable

physico-chemical, mechanical and thermal properties, that are suitable as alternative binders for the construction industry, fire/corrosion resistant materials or matrices for the encapsulation of hazardous elements [6–10]. Waste valorization results in minimization of the consumption of natural resources, reduction of the volume of wastes that are ultimately landfilled and reduction of the emissions of greenhouse gases (GHGs) [11–15].

Dredging operations in ports and rivers, in order to improve navigation, result in the excavation of big volumes of sediments that may often require special treatment and remediation [16]. In Europe, 100–200 Mm<sup>3</sup> of sediments are dredged annually to maintain efficiency in navigational waterways [17,18]. The management of sediments is an important issue and has several environmental and social implications [19]. The most important *ex situ* remediation technologies investigated so far include phytoremediation [20], electrokinetic remediation [21], bioleaching and stabilization [22–24] and development of technosols through composting [25].

Very interesting recent studies investigated the potential of calcination of marine sediments, in temperatures varying between 400 °C and 750 °C, for the subsequent production of geopolymer source materials and showed that increase of calcination temperature increases reactivity of the raw materials [26–29]. Other recent studies examined the use of different types of river and lake sediments for the production of bricks with high insulating capacity or aggregates which are suitable for cement

E-mail addresses: [komni@mred.tuc.gr](mailto:komni@mred.tuc.gr), [kostas.komnitsas@gmail.com](mailto:kostas.komnitsas@gmail.com) (K. Komnitsas).

mortars [30,31]. Liao et al. [32] investigated the potential of water reservoir sediments, mixed with sodium hydroxide, for the production of lightweight aggregates after calcination at higher temperature, ranging between 1045 °C and 1085 °C. Snellings et al. [33] investigated the effect of flash calcination of dredging sediments, carried out between 820 °C and 905 °C, on their properties and reactivity and mentioned that alternative supplementary cementitious materials (CSM) suitable for blended cements can be produced. In all these studies the pretreatment step of calcination, which results in increased energy consumption, is included. Thus, it will be interesting to explore in the near future cost and more energy efficient alternative routes for the valorization of marine sediments.

C&D wastes represent an important waste stream and huge quantities are produced every year in most countries [34–37]. The European Commission considers C&D wastes as priority waste stream for reuse and underlines their important environmental benefits as a result of their valorization [38]. C&D wastes are mainly used as recycled aggregates in concrete, as additives in cement production and as road base materials. The main factors that hinder the wider use of recycled C&D wastes in the construction industry include the lack of standards and specifications for recycled concrete production, the distance between demolition sites and recycling plants as well as lack of confidence from end users for the quality of the final products [39]. So far, studies have been carried out to investigate the potential of alkali activation of C&D wastes for the production of geopolymer binders and defined their properties and microstructure [40–43]. Recently, it has been shown that two of the components of C&D wastes namely bricks and tiles, which contain amorphous/semi-crystalline silica or aluminosilicate compounds, can be successfully alkali activated [44,45], while recycled demolition aggregates and crushed brick can be used for the production of geopolymers comprising calcium carbide residue, fly ash and slag as precursors [46] and ceramic sanitaryware as an alternative for the development of new sustainable binders [47].

The present experimental study aims to investigate the valorization of marine sediments and C&D wastes through alkali activation, define the morphology and determine the main factors that affect the properties of the final products. The study has a noticeable degree of novelty since so far very few studies are available in the international literature investigating valorization of marine sediments through alkali activation.

## 2. Materials and methodology

Marine sediments were collected from the ports of Souda in Chania, Crete, and Patras in NW Peloponnese, Greece. C&D waste components, including tiles, bricks and concrete, were collected from various demolished buildings of the city of Chania. Both sediments and C&D waste components were pulverized using a FRITSCH-BICO pulverizer (Germany) and homogenized. A Master-sizer S (Malvern Instruments) particle size analyzer was used for particle size analysis (Table 1). Table 2 shows the chemical composition, in the form of oxides, of sediments and each component of C&D wastes, as derived from an X-ray fluorescence energy dispersive spectrometer (Bruker-AXS S2 Ranger). Loss on

ignition (LOI) was determined by heating wastes at 1050 °C for 4 h. The weight percent of each raw material subjected to alkali activation as well as the codes of all specimens produced are presented in Table 3. The activating solution was prepared by dissolving the required amount of KOH pellets (Sigma Aldrich) in distilled water to obtain solution molarity 2–12 M and then adding sodium silicate solution ( $\text{Na}_2\text{SiO}_3$ , Merck,  $\text{Na}_2\text{O} = 7.5\text{--}8.5\%$ ,  $\text{SiO}_2 = 25.5\text{--}28.5\%$ ). The final solution was allowed to cool at room temperature for 24 h prior to use. The liquid/solid (L/S) ratio varied between 0.25 and 0.35 for each combination in order to improve the flowability characteristics of the resulting paste. An indicative composition of the starting mixture is (% weight): raw materials 82%,  $\text{H}_2\text{O}$  6%, KOH 3% and  $\text{Na}_2\text{SiO}_3$  9%.

The produced paste was cast in cubic metal moulds of 5 cm edge, which were vibrated for a few minutes to eliminate the presence of air voids in the reactive mass and improve the properties of the final solidified specimens. The moulds remained at room temperature for 2 h to allow early initiation of reactions, development of structural bonds and solidification of the paste. Then, the specimens were demoulded and sealed in plastic bags to prevent fast evaporation of water during curing and heated at 80 °C in a laboratory oven (ON-02G) for 24 h. After cooling and aging at room temperature for 7 days, compressive strength measurements were done using a MATEST C123N load frame. All tests and measurements were carried out in triplicate.

The morphology and structure of the final products was studied using analytical techniques. Fourier Transform Infrared Spectroscopy (FTIR) analysis was carried out, using pellets produced after mixing a pulverized sample of each specimen with KBr at a ratio of 1:100 w/w, with a Perkin-Elmer Spectrum 1000 spectrometer (USA). Scanning Electron Microscopy (SEM) analysis was performed with a JEOL 6380LV scanning electron microscope equipped with an EDS INCA microanalysis system with low vacuum, pressure 30 Pa, voltage 20 kV and 10–12 mm working distance from the detector. X-ray Diffraction (XRD) analysis of the raw materials and the produced specimens was performed using a Bruker AXS (D8 Advance type) diffractometer with Cu tube, scanning range from 4° to 70° 2 $\theta$ , step 0.02° and measuring time 0.2 s/step. The qualitative analysis was assessed with the use of the DIFFRAC<sup>plus</sup> EVA v. 2006 software and the Powder Diffraction File (PDF-2) database.

The thermal behaviour of the specimens was evaluated after heating them at 400, 600 or 800 °C for 1 h in a laboratory furnace N-8L Selecta. The structural integrity of selected specimens was assessed after immersing them in tap water and seawater for a period of up to 3 months or subjecting them to 20 freeze–thaw cycles, according to ASTM standard C1262-10 [48].

## 3. Results and discussion

### 3.1. Compressive strength

Fig. 1 shows the evolution of the compressive strength of the specimens produced from single wastes, namely C&D waste components (tiles, bricks and concrete), Patras sediments and Souda sediments vs KOH concentration. Specimen codes are given in Table 3, while error bars denote standard deviation of three specimens.

Regarding sediments, it is seen from this data that only Patras sediments can be alkali activated. The compressive strength of the produced specimens increases from 8.5 to 19 MPa when KOH molarity increases from 2 to 4 M, while further increase of molarity (6 to 12 M) has no additional beneficial effect. Souda sediments are only slightly alkali activated (maximum compressive strength is 5 MPa). This is mainly due to their lower content of  $\text{SiO}_2$  which reduces the molar ratio of  $\text{SiO}_2/\text{Al}_2\text{O}_3$  (4.5 compared to the

**Table 1**  
Particle size of the raw materials.

|                            | Souda sediments | Patras sediments | Tiles | Bricks | Concrete |
|----------------------------|-----------------|------------------|-------|--------|----------|
| size ( $\mu\text{m}$ )     | <120            | <120             | <140  | <140   | <190     |
| $d_{50}$ ( $\mu\text{m}$ ) | 9               | 8                | 14    | 7      | 10       |

**Table 2**  
Chemical composition (% weight) of the raw materials.

|                  | SiO <sub>2</sub> | Al <sub>2</sub> O <sub>3</sub> | CaO   | Fe <sub>2</sub> O <sub>3</sub> | Na <sub>2</sub> O | MgO  | K <sub>2</sub> O | MnO  | P <sub>2</sub> O <sub>5</sub> | SO <sub>3</sub> | TiO <sub>2</sub> | LOI   | SUM    |
|------------------|------------------|--------------------------------|-------|--------------------------------|-------------------|------|------------------|------|-------------------------------|-----------------|------------------|-------|--------|
| Souda sediments  | 29.10            | 6.49                           | 24.50 | 3.62                           | 0.09              | 1.34 | 0.68             | 0.03 | 0.31                          | 1.10            | 0.38             | 29.20 | 96.80  |
| Patras sediments | 37.10            | 4.97                           | 21.30 | 2.63                           | 1.16              | 1.55 | 1.41             | 0.10 | 0.09                          | 0.62            | 0.34             | 27.34 | 98.61  |
| Tiles            | 70.54            | 9.80                           | 8.78  | 5.39                           | –                 | 4.46 | 1.37             | 0.06 | –                             | –               | 0.77             | 0.23  | 101.41 |
| Bricks           | 57.79            | 14.95                          | 8.79  | 6.00                           | 1.03              | 4.75 | 2.80             | 0.05 | 0.23                          | –               | 0.85             | 1.89  | 99.12  |
| Concrete         | 5.81             | 1.49                           | 65.42 | 0.75                           | 0.57              | 4.21 | 1.26             | 0.01 | 0.73                          | 0.82            | 0.03             | 21.59 | 102.68 |

**Table 3**  
% weight of each raw material subjected to alkali activation.

| Code           | Tiles    | Bricks   | Concrete | Souda sediments | Patras sediments |
|----------------|----------|----------|----------|-----------------|------------------|
| T              | 100      | –        | –        | –               | –                |
| B              | –        | 100      | –        | –               | –                |
| C              | –        | –        | 100      | –               | –                |
| SS             | –        | –        | –        | 100             | –                |
| TSS10 or TSS30 | 90 or 70 | –        | –        | 10 or 30        | –                |
| BSS10 or BSS30 | –        | 90 or 70 | –        | 10 or 30        | –                |
| CSS10 or CSS30 | –        | –        | 90 or 70 | 10 or 30        | –                |
| PS             | –        | –        | –        | –               | 100              |
| TPS10 or TPS30 | 90 or 70 | –        | –        | –               | 10 or 30         |
| BPS10 or BPS30 | –        | 90 or 70 | –        | –               | 10 or 30         |
| CPS10 or CPS30 | –        | –        | 90 or 70 | –               | 10 or 30         |

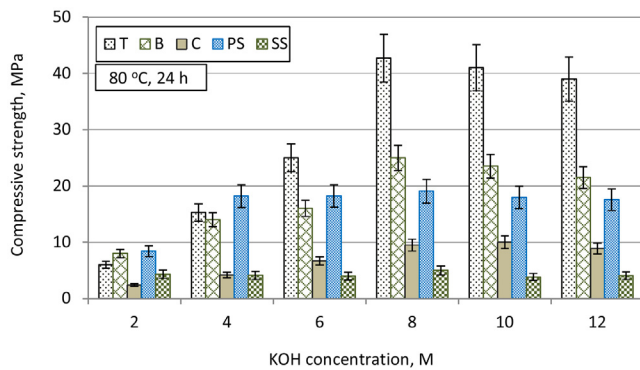


**Fig. 1.** Evolution of the compressive strength of specimens produced from tiles, bricks, concrete, Patras sediments and Souda sediments vs KOH concentration (specimen codes are given in Table 3).

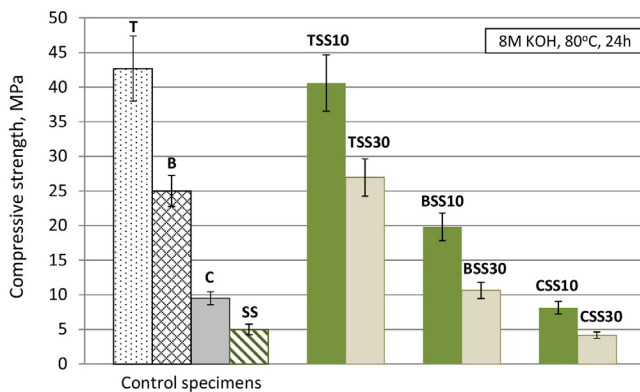


**Fig. 2.** Compressive strength of tile-, brick- and concrete-based specimens when 10 or 30% w/w of Souda sediments are added (specimen codes are presented in Table 3).

respective 7.5 ratio for Patras sediments) and does not allow the solubilization of sufficient amounts of Si and Al and the formation of aluminosilicate bonds which contribute to the development of matrices with higher compressive strength. Another reason may be the presence of more amorphous silica compounds in Patras sediments which assist the evolution of geopolymerisation reactions.

Regarding C&D waste components, tiles exhibit the best alkali activation potential and under the optimum KOH molarity (8 M) the compressive strength of the specimens reached 42.7 MPa. A similar behaviour is shown for brick-based specimens which acquire though lower strength (up to 25 MPa). For both tile- and brick-based specimens, the strength increase is related to the increase of KOH molarity which accelerates alkali activation reactions and thus enhances dissolution of Si and Al from the raw materials. On the other hand, concrete exhibits lower alkali activation potential (maximum compressive strength acquired is 9.5 MPa). This is due to its low content of SiO<sub>2</sub> and Al<sub>2</sub>O<sub>3</sub> (5.81% and 1.49%, respectively) as well as its high content of CaO (65.42%), which consumes KOH rendering it insufficient for the dissolution of aluminosilicates from the raw materials [44].

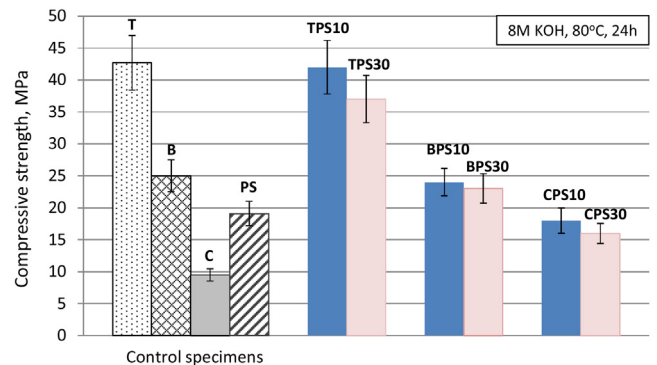


**Fig. 3.** Compressive strength of tile-, brick- and concrete-based specimens when 10 or 30% w/w of Patras sediments are added (specimen codes are presented in Table 3).

**Table 4**

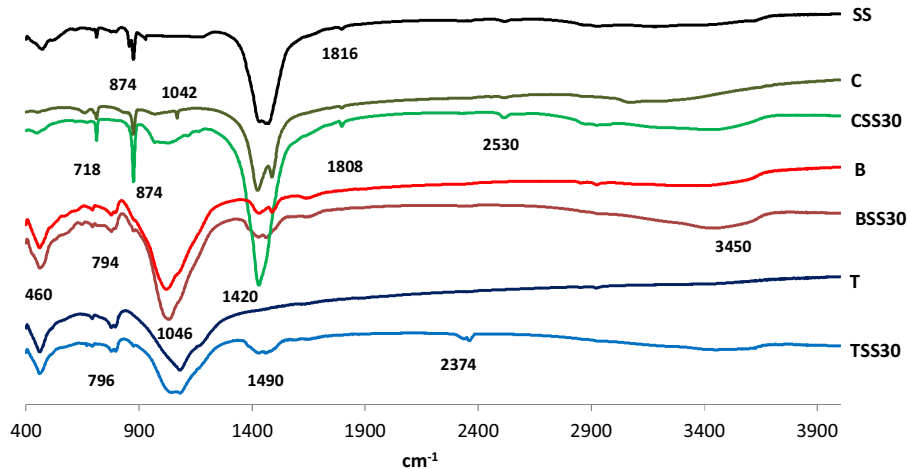
Molar ratios of oxides of the initial paste and compressive strength of selected specimens (8 M KOH).

| Code  | SiO <sub>2</sub>               |  | SiO <sub>2</sub>   | H <sub>2</sub> O                       | Strength (MPa) |
|-------|--------------------------------|--|--|--|----------------|
|       | Al <sub>2</sub> O <sub>3</sub> | (Al <sub>2</sub> O <sub>3</sub> + CaO) | (Al <sub>2</sub> O <sub>3</sub> + Fe <sub>2</sub> O <sub>3</sub> ) | (Na <sub>2</sub> O + K <sub>2</sub> O) |                |
| T     | 12.57                          | 4.78                                   | 9.31   | 10.42                                  | 42.7           |
| B     | 6.83                           | 3.30                                   | 5.44   | 8.30                                   | 25             |
| C     | 9.01                           | 0.11                                   | 6.82   | 9.76                                   | 9.5            |
| SS    | 5.85                           | 0.56                                   | 5.85   | 9.59                                   | 5              |
| TSS30 | 11.43                          | 2.91                                   | 8.46   | 10.05                                  | 27             |
| BSS30 | 6.74                           | 0.17                                   | 2.22   | 5.32                                   | 10.6           |
| CSS30 | 7.47                           | 0.18                                   | 5.59   | 10.06                                  | 4.2            |
| PS    | 13.47                          | 1.53                                   | 13.47  | 9.08                                   | 19.1           |
| TPS30 | 12.40                          | 3.68                                   | 5.87   | 10.08                                  | 37             |
| BPS30 | 7.42                           | 0.14                                   | 2.77   | 5.87                                   | 23             |
| CPS30 | 11.37                          | 0.25                                   | 8.57   | 9.80                                   | 16.5           |

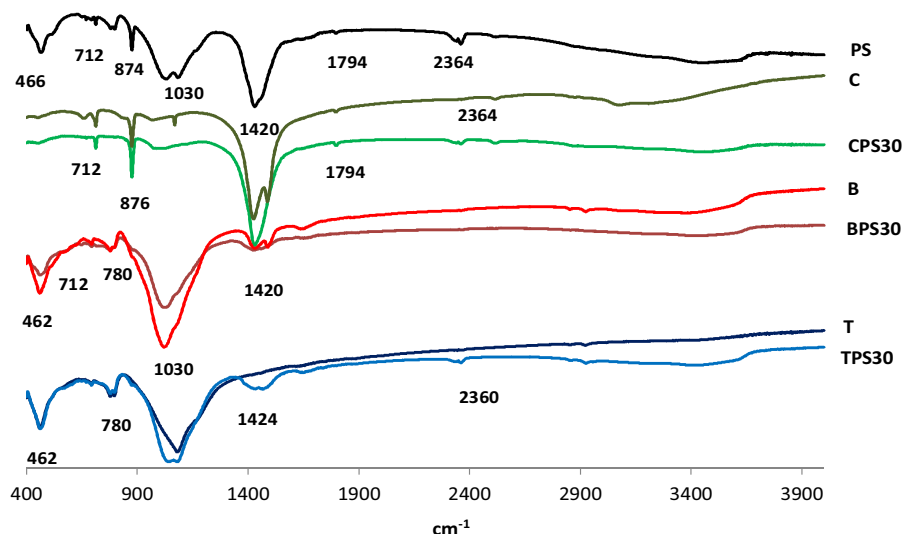
The compressive strength of the produced specimens when tiles, bricks and concrete were mixed with 10 or 30% w/w of Souda or Patras sediments, as well as of the control specimens prepared from single raw materials, is shown in Figs. 2 and 3, respectively. Specimens were prepared with 8 M KOH based on the results of

Fig. 1. Table 4 shows the molar ratios of the oxides present in the initial paste.

According to Fig. 2, when tiles, bricks and concrete are mixed with 10% w/w Souda sediments, the produced specimens show a slightly decreased compressive strength compared to the respective control specimens prepared from single C&D waste components. A noticeable further decrease in strength is shown when the Souda sediments addition percentage increases to 30% w/w. This behaviour can be explained by the decrease of SiO<sub>2</sub>/Al<sub>2</sub>O<sub>3</sub> and SiO<sub>2</sub>/(Al<sub>2</sub>O<sub>3</sub> + CaO) ratios in the initial C&D waste component–sediment mixture. For example, when tiles are mixed with 30% w/w Souda sediments (TSS30) these ratios are 11.43 and 2.91, respectively, while when tiles are only used as raw materials both ratios and especially the second one are higher (12.57 and 4.78, respectively). A similar trend is shown for brick- and cement-based specimens. Specimens with high compressive strength are usually obtained when high SiO<sub>2</sub>/Al<sub>2</sub>O<sub>3</sub> and SiO<sub>2</sub>/(Al<sub>2</sub>O<sub>3</sub> + CaO) molar ratios are present in the initial paste, as discussed in a recent study [44]. In case the SiO<sub>2</sub>/Al<sub>2</sub>O<sub>3</sub> ratio is low, such as in SS specimen (5.85), the number of aluminosilicate bonds is lower and specimens acquire low final strength (5 MPa), as also shown in other studies [49,50].



**Fig. 4.** FTIR spectra of selected specimens produced from C&D wastes, Souda sediments and their combinations (C&D wastes with 30% w/w sediment).



**Fig. 5.** FTIR spectra of selected specimens produced from C&D wastes, Patras sediments and their combinations (C&D wastes with 30% w/w sediment).

**Table 5**  
FTIR spectra band assignments.

| Band number, $\text{cm}^{-1}$ | Assignment   | References |
|-------------------------------|--|------------|
| 3450, 2300–2500, 1800         | H—O—H stretching and bending vibrations  | [51,52]    |
| 1490, 1420, 874               | Atmospheric carbonation, out of plane bending of $\text{CO}_3$                           | [53]       |
| 1050                          | Si—O stretching vibrations and Si—O—Si or Al—O—Si asymmetric stretching vibrations       | [54,55]    |
| 460–800                       | In plane Si—O bending and Al—O linkages as well as bending Si—O—Si and O—Si—O vibrations | [56]       |

It is shown from Fig. 3, that when tiles or bricks are mixed with 10% w/w of Patras sediments, the produced specimens (TPS10 or BPS10) acquire a slightly lower strength compared to the control tile- or brick- based specimens, respectively. When the Patras sediments addition percentage increases to 30% w/w strength decreases further but still remains at acceptable values, 37 and 23 MPa for TPS30 and BPS30 specimens, respectively. As shown in

Table 4 the values of  $\text{SiO}_2/\text{Al}_2\text{O}_3$  ratio in the initial mixtures are quite similar for specimens acquiring high strength, namely 12.57 for T specimen and 12.40 for TPS30 specimen.

When concrete is mixed with 10% w/w Patras sediments, the strength of CPS10 specimen is 18 MPa and is almost double compared to the strength of concrete-control specimen (9.5 MPa). A slight further decrease of strength to 16.5 MPa is recorded when

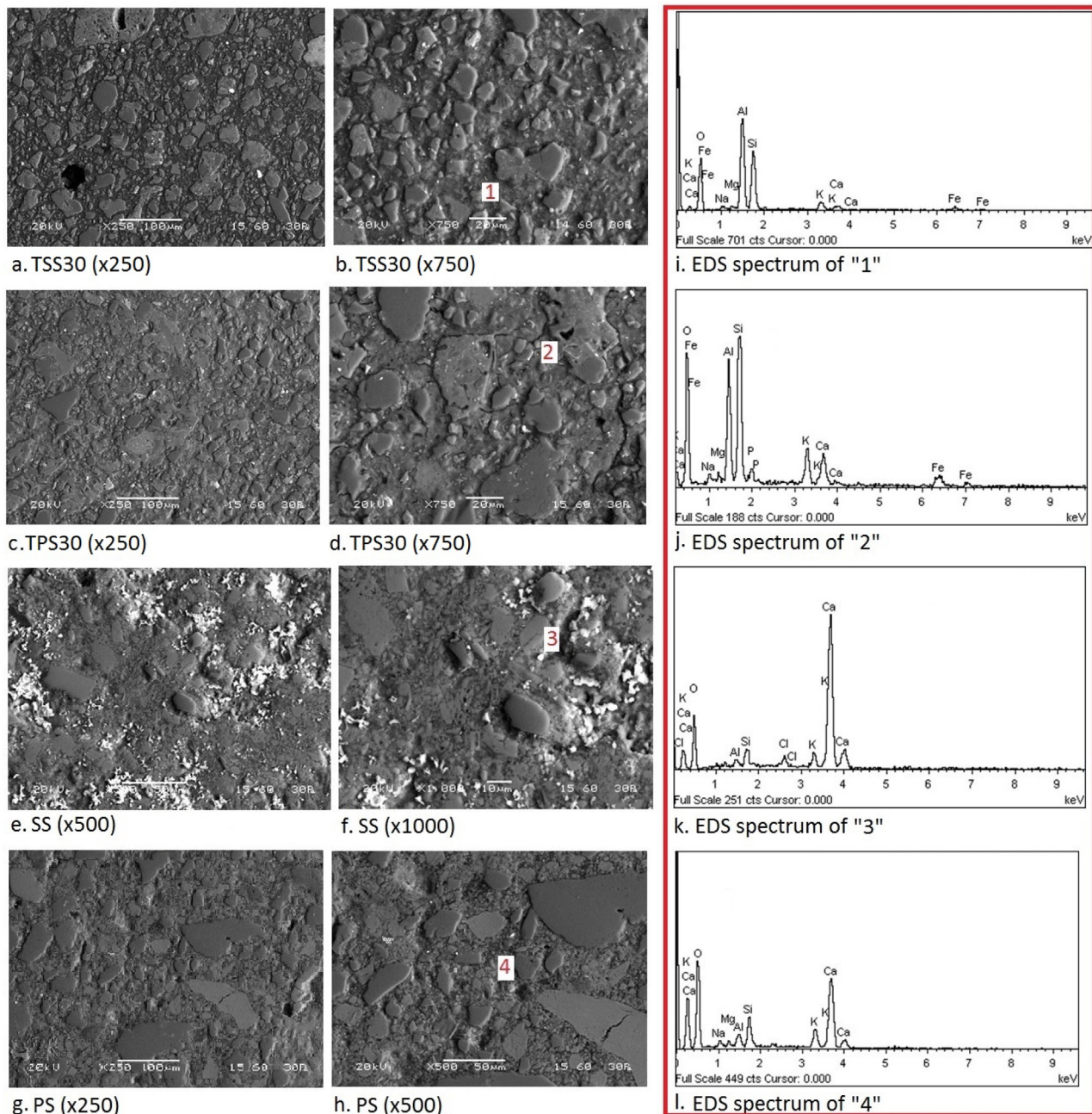


**Fig. 6.** SEM images of selected specimens produced from Souda or Patras sediments and their combination with tiles.

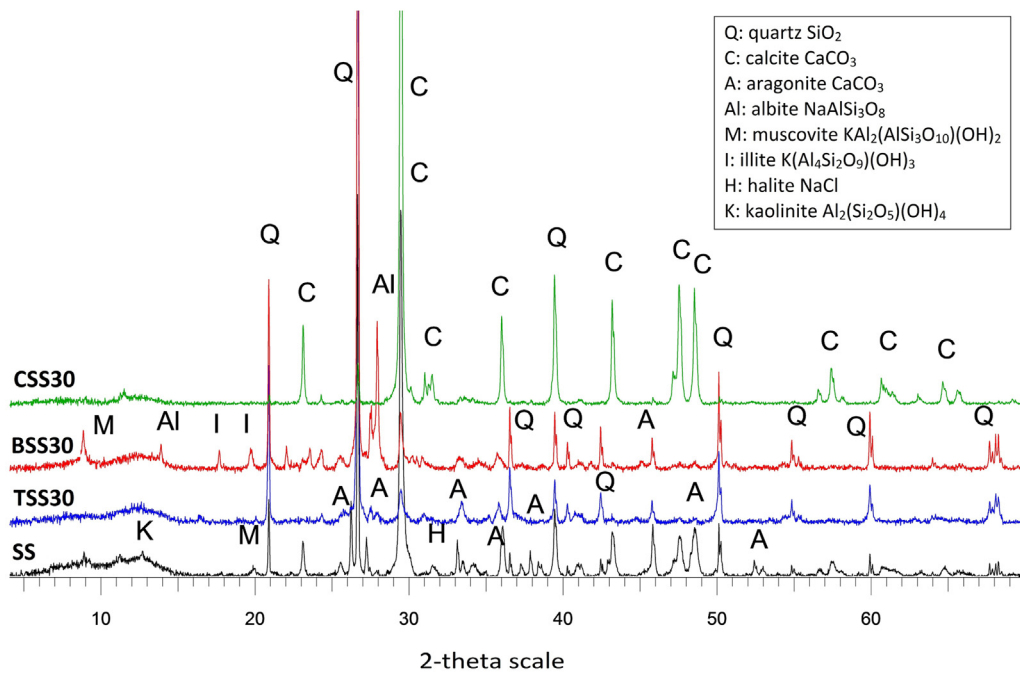


Fig. 7. XRD patterns of specimens produced from Souda sediments and their combination with C&D waste components (specimen codes are presented in Table 3).

the addition percentage of Patras sediments increases to 30% w/w (CPS30 specimen). This result is related with the lower compressive strength values obtained when the respective single components were alkali activated.

Other molar ratios such as  $\text{SiO}_2/(\text{Al}_2\text{O}_3 + \text{Fe}_2\text{O}_3)$  and  $\text{H}_2\text{O}/(\text{Na}_2\text{O} + \text{K}_2\text{O})$  may be considered to elucidate the role of the mineralogy of the raw materials during alkali activation. As shown in Table 4, if the molar ratios  $\text{SiO}_2/(\text{Al}_2\text{O}_3 + \text{Fe}_2\text{O}_3)$  and  $\text{SiO}_2/\text{Al}_2\text{O}_3$  are low (e.g. 2.22 and 6.74 for the BSS30 paste, respectively) the final specimen also acquires low compressive strength (10.6 MPa). When both these ratios are increased, as shown in the starting

mixture used for the preparation of the TSS30 specimen (8.46 and 11.43, respectively), the compressive strength also increases (27 MPa). Finally, it has to be mentioned that the ratio  $\text{H}_2\text{O}/(\text{Na}_2\text{O} + \text{K}_2\text{O})$  is higher than 5 in all starting mixture combinations, indicating that sufficient water is available in the reactive paste to allow initiation of alkali activation reactions.

### 3.2. Mineralogy and morphology

Fig. 4 shows the FTIR spectra of specimens produced using C&D wastes, Souda sediments and their combinations. Quite similar

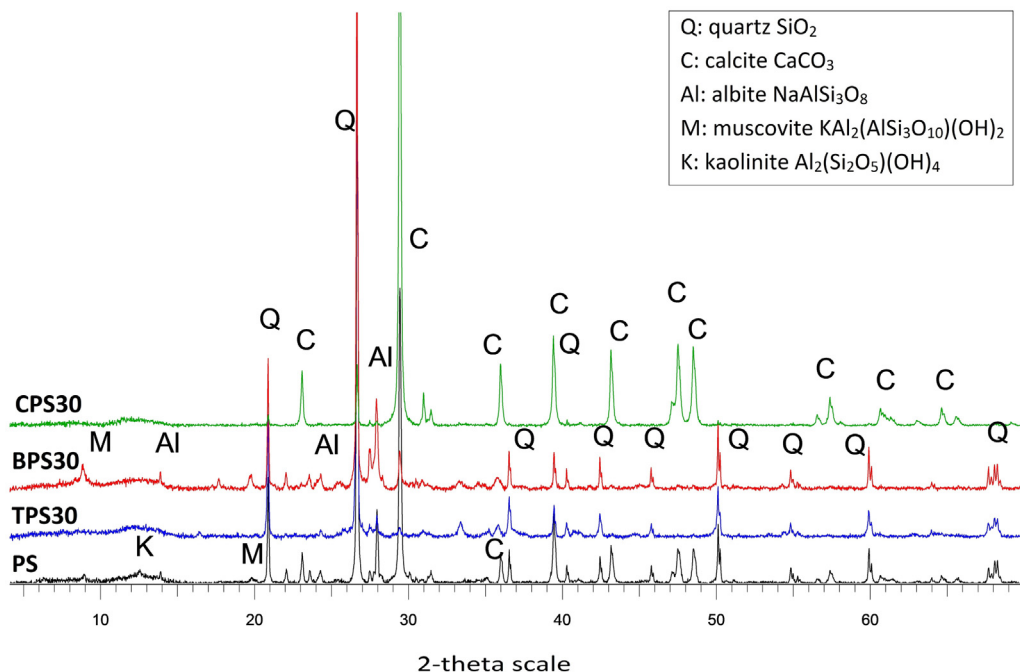


Fig. 8. XRD patterns of specimens produced from Patras sediments and their combination with C&D waste components (specimen codes are presented in Table 3).

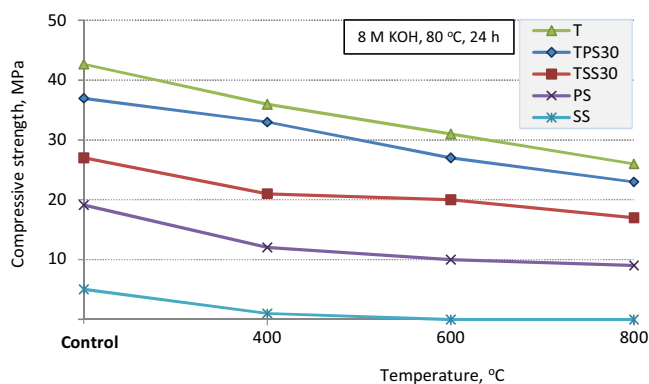


Fig. 9. Compressive strength of selected specimens subjected to high temperature heating.

FTIR spectra are shown for specimens produced using C&D wastes and Patras sediments (Fig. 5). The respective spectra band assignments are summarized in Table 5. The small bands detected in the region of  $3450\text{ cm}^{-1}$ ,  $2300\text{--}2500\text{ cm}^{-1}$  and around  $1800\text{ cm}^{-1}$  are assigned to stretching and bending H—O—H vibrations of bound water molecules. The doublet of peaks seen at  $1490$  and  $1420\text{ cm}^{-1}$  for all specimens, except for T, is due to atmospheric carbonation. The band at  $1420\text{ cm}^{-1}$  is quite strong in specimens that have a high  $\text{CaCO}_3$  content (C, SS, CSS30, PS, CPS30) and is attributed to the modes of  $\text{CO}_3$ . The sharp peak at  $874\text{ cm}^{-1}$  is also assigned to out of plane bending of  $\text{CO}_3$  and shown only in these specimens. The broad peaks at around  $1050\text{ cm}^{-1}$  are major fingerprints of the geopolymeric aluminosilicate matrix and are attributed to Si—O stretching vibrations of  $\text{SiO}_4$  and Si—O—Si or Al—O—Si asymmetric stretching vibrations during alkali activation. This peak is barely shown in SS, C and CSS30 specimens that acquire strength lower than 10 MPa. The bands at around  $460\text{--}800\text{ cm}^{-1}$  are due to Si—O, Al—O, Si—O—Si and O—Si—O vibrations.

In Fig. 6, SEM images of selected specimens produced using Soda or Patras sediments and their combination with tiles, the C&D waste component with the highest alkali activation potential, are illustrated. The matrix of TSS30 (Fig. 6a,b) and TPS30 specimens (Fig. 6c,d) is more homogeneous compared to SS (Fig. 6e,f) and PS specimens (Fig. 6g,h), respectively, indicating sufficient reaction of the raw materials during alkali activation. As also deduced from EDS analysis of TSS30 and TPS30 specimens (Fig. 6i,j, respectively) which acquire strength of 27 and 37 MPa, respectively, the content

of Si and Al which are the main elements required for alkali activation, is high, indicating that Si—O—Al bonds are present in the developed matrix. In SS specimen, Fig. 6k, Ca is the main component, Cl is detected in the white areas, while Si and Al are found in smaller quantities. In the EDS spectrum of PS specimen, Fig. 6l, Ca is present while also some Si and Al which have been dissolved from Patras sediments are detected.

Figs. 7 and 8 present the XRD patterns of selected specimens. As deduced from these figures, specimens consist of partially reacted or unreacted crystalline phases, such as quartz, calcite, albite, muscovite, kaolinite and halite which were also present in the raw materials. In specimens that acquire higher compressive strength, for example TPS30 and TSS30, higher Si and Al solubilization from the raw materials takes place that results in the formation of aluminosilicate gel and subsequent hardening, in accordance with the EDS spectra (Fig. 6i,j). On the other hand, mainly unreacted crystalline phases are present in the XRD patterns of specimens acquiring low strength, eg. SS and CSS30. It is also shown that specimens acquiring high compressive strength are characterized by a certain degree of amorphicity [57].

### 3.3. Structural integrity

Fig. 9 presents the compressive strength of selected specimens subjected to high temperature heating at 400, 600 and  $800\text{ }^\circ\text{C}$  for one hour. The compressive strength of the control specimens, which were not subjected to high temperature heating, is also given for comparison. It is evident that for all specimens, strength decreases gradually when temperature increases from 400 to  $800\text{ }^\circ\text{C}$ . The best behaviour is shown for T specimens, produced only from tiles, while specimen TPS30 produced from tiles and 30% w/w Patras sediments also exhibits good structural integrity. Despite the fact that the strength of both T and TPS30 specimens decreases significantly (almost 40%) after heating at  $800\text{ }^\circ\text{C}$ , compared to the respective controls, it still remains at acceptable values (higher than 22 MPa) indicating their potential use as structural or fire-protection materials. TSS30 and PS specimens acquire lower strength after heating at  $800\text{ }^\circ\text{C}$  (17 and 9 MPa, respectively), while SS specimens totally decompose after heating at relatively low temperature ( $400\text{ }^\circ\text{C}$ ).

The strength decrease after high temperature heating is mainly caused by the decomposition of aluminosilicate bonds and the resulting deterioration of structural integrity of the specimens, as is also seen by the development of cracks and discussed in other recent studies [58,59].

Fig. 10 shows the compressive strength of TPS30 and TSS30 specimens immersed in tap water or seawater for a maximum

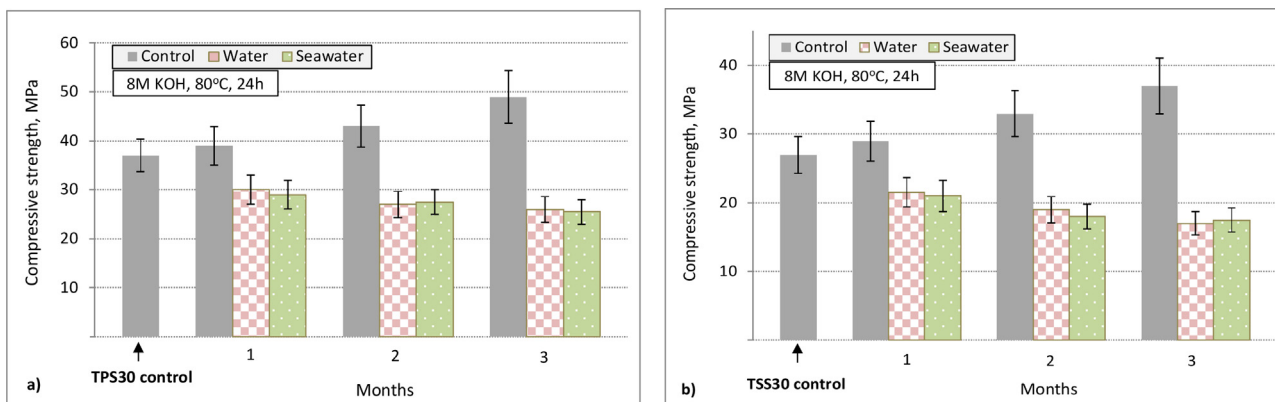


Fig. 10. Compressive strength of (a) TPS30 and (b) TSS30 specimens immersed in water or seawater for a maximum period of 3 months.

period of 3 months; the compressive strength of control specimens is also shown for comparison and gradually increases with time.

It is shown that TPS30 (Fig. 10a) and TSS30 specimens (Fig. 10b) have quite similar behaviour when immersed in water or seawater; however, the strength is higher for TPS30 specimens. In both tests the strength decreases by almost 25% after 1 month compared to the respective controls and it is slightly affected after 2 or 3 months of immersion. The lower strength obtained after 3 months is 25 and 17 MPa, for TPS30 and TSS30 specimens, respectively. Fig. 11 shows that the strength of the specimens subjected to 20 freeze-thaw cycles, according to ASTM standard C1262-10, is decreased by 16 and 22%, for TPS30 and TSS30 specimens, respectively, compared to the controls. It is deduced from these results that the integrity of the specimens is negatively affected mainly by the de-polymerisation of the alumino-silicate matrix in extreme temperature conditions or after water absorption during immersion.

Finally, it is mentioned that the anticipated leaching of hazardous constituents, mainly heavy metals, from the produced specimens is very low, given the fact that their degree of solubilisation from the initial raw materials is negligible to low, as indicated in earlier studies [16,44].

#### 4. Conclusions

C&D waste components, namely tiles or bricks, can be alkali activated under the optimum activating solution molarity (8–12 M KOH) and their compressive strength reaches 43 and 25 MPa, respectively. On the other hand, concrete acquires a maximum compressive strength of almost 10 MPa due to its low  $\text{SiO}_2$ ,  $\text{Al}_2\text{O}_3$  and high CaO content. Sediments from Patras port can be alkali activated (compressive strength up to 20 MPa) for the production of building materials, while specimens produced from Souda sediments acquire lower strength, around 5 MPa.

However, both sediments can be co-utilized with tiles or bricks (weight ratio marine sediments: tiles or bricks 10:90 or 30:70), for the production of specimens with compressive strength up to 42 MPa using 8 M KOH as alkali activator. Specimens with high compressive strength are obtained when high  $\text{SiO}_2/\text{Al}_2\text{O}_3$  and  $\text{SiO}_2/(\text{Al}_2\text{O}_3 + \text{CaO})$  molar ratios are present in the initial paste, namely 12.40 and 3.68, respectively, such as those calculated for TPS30 specimen produced using tiles and 30% w/w Patras sediments. When the ratio  $\text{SiO}_2/\text{Al}_2\text{O}_3$  is low, as it happens for Souda sediments, the formation of alumino-silicate bonds is limited and low final strength is acquired.

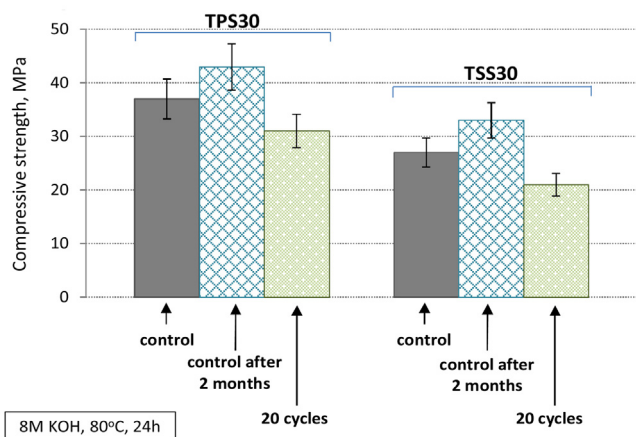


Fig. 11. Compressive strength of TPS30 and TSS30 specimens subjected to freeze-thaw cycles according to ASTM standard C1262-10.

Analytical techniques, namely Fourier Transform Infrared Spectroscopy (FTIR), Scanning Electron Microscopy (SEM) and X-ray Diffraction (XRD), were used for the identification of the morphology of the final products. It was shown that the strongest inorganic polymer bonds are developed in specimens acquiring high strength, such as T, B, TPS30 and TSS30, when sufficient number of Si and Al ions is solubilized during alkali activation of the raw materials. Thus Si–O–Si and Al–O–Si bonds are formed while the matrix of these specimens is homogeneous. Unreacted crystalline phases are present in specimens acquiring low strength, as for example in those produced using Souda sediments or mixtures with concrete, indicating limited solubilization of Si and Al from the raw materials.

Specimens acquiring high strength, such as those produced from tiles or mixtures of tiles and Patras sediments, show good structural integrity during heating up to 800 °C, immersion in water or seawater and freeze-thaw cycles, indicating their potential use as structural or fire-protection components.

#### Acknowledgements

The authors would like to acknowledge the financial support of European Commission in the frame of Horizon 2020 project “Metal recovery from low-grade ores and wastes”, [www.metgrowplus.eu](http://www.metgrowplus.eu), Grant Agreement n° 690088.

#### References

- [1] K. Komnitsas, D. Zaharaki, Geopolymerisation: a review and prospects for the minerals industry, *Miner. Eng.* 20 (2007) 1261–1277.
- [2] J. Davidovits, Geopolymers: inorganic polymeric new materials, *J. Mater. Educ.* 16 (1994) 91–139.
- [3] K. Komnitsas, D. Zaharaki, G. Bartzas, Effect of sulphate and nitrate anions on heavy metal immobilisation in ferronickel slag geopolymers, *Appl. Clay Sci.* 73 (2013) 103–109.
- [4] F. Pacheco-Torgal, Z. Abdollahnejad, A.F. Camões, M. Jamshidi, Y. Ding, Durability of alkali-activated binders: a clear advantage over Portland cement or an unproven issue? *Constr. Build. Mater.* 30 (2012) 400–405.
- [5] L.K. Turner, F.G. Collins, Carbon dioxide equivalent ( $\text{CO}_2\text{-e}$ ) emissions: a comparison between geopolymer and OPC cement concrete, *Constr. Build. Mater.* 43 (2013) 125–130.
- [6] S.A. Bernal, E.D. Rodríguez, A.P. Kirchheim, J.L. Provis, Management and valorisation of wastes through use in producing alkali-activated cement materials, *J. Chem. Technol. Biotechnol.* (2016), doi:<http://dx.doi.org/10.1002/jctb.4927>.
- [7] A. Nazer, J. Payá, M.V. Borrachero, J. Monzó, Use of ancient copper slags in Portland cement and alkali activated cement matrices, *J. Environ. Manage.* 167 (2016) 115–123.
- [8] J.L. Provis, P. Duxson, J.S.L. Van Deventer, The role of particle technology in developing sustainable construction materials, *Adv. Powder Technol.* 21 (2007) 2–7.
- [9] B. Singh, G. Ishwarya, M. Gupta, S.K. Bhattacharyya, Geopolymer concrete: A review of some recent developments, *Constr. Build. Mater.* 85 (2015) 78–90.
- [10] J. Yliniemi, J. Pesonen, M. Tiainen, M. Ilikainen, Alkali activation of recovered fuel–biofuel fly ash from fluidised-bed combustion: stabilisation/solidification of heavy metals, *Waste Manage.* 43 (2015) 273–282.
- [11] M. Bravo, J. De Brito, J. Pontes, L. Evangelista, Mechanical performance of concrete made with aggregates from construction and demolition waste recycling plants, *J. Clean. Prod.* 99 (2015) 59–74.
- [12] H. Dahlbo, J. Bachér, K. Lähtinen, P. Jouttijärvi, T. Suoheimo, S. Mattila, T. Sironen, K. Saramäki, Construction and demolition waste management: a holistic evaluation of environmental performance, *J. Clean. Prod.* 107 (2015) 333–341.
- [13] P. Duxson, J.L. Provis, G.C. Lukey, J.S.J. van Deventer, The role of inorganic polymer technology in the development of ‘green concrete’, *Cem. Concr. Res.* 37 (2007) 1590–1597.
- [14] G. Habert, J.B. d’Espinoze de Lacaillerie, N. Roussel, An environmental evaluation of geopolymer based concrete production: reviewing current research trends, *J. Clean. Prod.* 19 (2011) 1229–1238.
- [15] K. Komnitsas, Potential of geopolymer technology towards green buildings and sustainable cities, *Procedia Eng.* 21 (2011) 1023–1032.
- [16] K. Komnitsas, I. Pyltiotis, D. Zaharaki, E. Manoutsoglou, Using various guidelines and approaches for the assessment of marine sediment quality, *Environ. Forensics* 16 (2015) 109–116.
- [17] M.L. Alonso Castillo, I. Sanchez Trujillo, E. Vereda Alonso, A. Garcia de Torres, J. M. Cano Pavon, Bioavailability of heavy metals in water and sediments from a

- typical Mediterranean Bay (Malaga Bay, Region of Andalucia, Southern Spain), *Mar. Pollut. Bull.* 76 (2013) 427–434.
- [18] S.F. Goncalves, R. Calado, N.C.M. Gomes, A.M.V.M. Soares, S. Loureiro, An ecotoxicological analysis of the sediment quality in a European Atlantic harbor emphasizes the current limitations of the Water Framework Directive, *Mar. Pollut. Bull.* 72 (2013) 197–204.
- [19] M.E. Bates, C. Fox-Lent, L. Seymour, B.A. Wender, I. Linkov, Life cycle assessment for dredged sediment placement strategies, *Sci. Total Environ.* 511 (2015) 309–318.
- [20] G. Masciandaro, C. Di Biase, E. Macci, R. Peruzzi, S. Doni, Phytoremediation of dredged marine sediment: monitoring of chemical and biochemical processes contributing to sediment reclamation, *J. Environ. Manage.* 134 (2014) 166–174.
- [21] M.T. Ammami, F. Portet-Koltalo, A. Benamar, C. Duclairoir-Poc, H. Wang, F. Le Derf, Application of biosurfactants and periodic voltage gradient for enhanced electrokinetic remediation of metals and PAHs in dredged marine sediments, *Chemosphere* 125 (2015) 1–8.
- [22] A. Akcil, C. Erust, S. Ozdemiroglu, V. Fonti, F. Beolchini, A review of approaches and techniques used in aquatic contaminated sediments: metal removal and stabilization by chemical and biotechnological processes, *J. Clean. Prod.* 86 (2015) 24–36.
- [23] V. Fonti, A. Antonio Dell'Anno, F. Beolchini, Does bioleaching represent a biotechnological strategy for remediation of contaminated sediments? *Sci. Tot. Environ.* 563–564 (2016) 302–319.
- [24] P. Mattei, L.P. D'Acqui, F.P. Nicese, G. Lazzarini, G. Masciandaro, C. Macci, S. Doni, F. Sarteschi, L. Giagnoni, G. Renella, Use of phytoremediated sediments dredged in maritime port as plant nursery growing media, *J. Environ. Manage.* (2016). <http://dx.doi.org/10.1016/j.jenvman.2016.05.069>.
- [25] P. Macía, C. Fernández-Costas, P. Rodríguez, M. Sieiro, M.A. Sanromán, Technosols as a novel valorization strategy for an ecological management of dredged marine sediments, *Ecol. Eng.* 67 (2014) 182–189.
- [26] C. Ferone, F. Colangelo, R. Cioffi, F. Montagnaro, L. Santoro, Use of reservoir clay sediments as raw materials for geopolymer binders, *Adv. Appl. Ceram.* 112 (2013) 184–189.
- [27] C. Ferone, B. Liguori, I. Capasso, F. Colangelo, R. Cioffi, E. Cappelleto, R. Di Maggio, Thermally treated clay sediments as geopolymer source material, *Appl. Clay Sci.* 107 (2015) 195–204.
- [28] B. Molino, A. Vincenzo, C. Ferone, F. Messina, F. Colangelo, R. Cioffi, Recycling of clay sediments for geopolymer binder production. A new perspective for reservoir management in the framework of Italian legislation: the Occhito reservoir case study, *Materials* 7 (2014) 5603–5616.
- [29] S. Peirce, L. Santoro, S. Andini, F. Montagnaro, C. Ferone, R. Cioffi, Clay sediment geopolymerization by means of alkali metal aluminate activation, *RSC Adv.* 130 (2015) 107662–107669.
- [30] J. Couvidat, M. Benzazoua, V. Chatain, A. Bouamrane, H. Bouzahzah, Feasibility of the reuse of total and processed contaminated marine sediments as fine aggregates in cemented mortars, *Constr. Build. Mater.* 112 (2016) 892–902.
- [31] Y. Xu, C. Yan, B. Xu, X. Ruan, Z. Wei, The use of urban river sediments as a primary raw material in the production of highly insulating brick, *Ceram. Int.* 40 (2014) 8833–8840.
- [32] Y.-C. Liao, C.-Y. Huang, Y.-M. Chen, Lightweight aggregates from water reservoir sediment with added sodium hydroxide, *Constr. Build. Mater.* 46 (2013) 79–85.
- [33] R. Snellings, Ö. Cizer, L. Horckmans, P.T. Durdziński, P. Dierckx, P. Nielsen, K. Van Balen, L. Vandewalle, Properties and pozzolanic reactivity of flash calcined dredging sediments, *Appl. Clay Sci.* 129 (2016) 35–39.
- [34] T. Ding, J. Xiao, Estimation of building-related construction and demolition waste in Shanghai, *Waste Manag.* 34 (2014) 2327–2334.
- [35] D.H.F. Paz, K.P.V. Lafayette, Forecasting of construction and demolition waste in Brazil, *Waste Manage. Res.* 34 (2016) 708–716.
- [36] U.A. Umar, A. Shafiq, M.F. Nuruddin, M.F. Khamidi, A review on adoption of novel techniques in construction waste management and policy, *J. Mater. Cycles Waste* (2016), doi:<http://dx.doi.org/10.1007/s10163-016-0534-8>.
- [37] Z. Wu, A.T.W. Yu, L. Shen, G. Liu, Quantifying construction and demolition waste: an analytical review, *Waste Manage.* 34 (2014) 1683–1692.
- [38] Directive 2008/98/EC of the European Parliament and of the Council on waste and repealing certain Directives, 19 Nov. 2008, Official Journal of the European Union, L312/3.
- [39] D.X. [39], A.A.A. Xuan, L.J.M. Molenaar, Houben Evaluation of cement treatment of reclaimed construction and demolition waste as road bases, *J. Clean. Prod.* 100 (2015) 77–83.
- [40] A. Allahverdi, E.N. Kani, Construction wastes as raw materials for geopolymer binders, *Int. J. Civil Eng.* 7 (2009) 154–160.
- [41] A. Pathak, S. Kumar, V.K. Jha, Development of building material from geopolymerization of construction and demolition waste (CDW), *Trans. Indian Ceram. Soc.* 73 (2014) 133–137.
- [42] L. Reig, M.M. Tashima, M.V. Borrachero, J. Monzó, C.R. Cheeseman, J. Payá, Properties and microstructure of alkali-activated red clay brick waste, *Constr. Build. Mater.* 43 (2013) 98–106.
- [43] Z. Sun, H. Cui, H. An, D. Tao, Y. Xu, J. Zhai, Q. Li, Synthesis and thermal behavior of geopolymer-type material from waste ceramic, *Constr. Build. Mater.* 49 (2013) 281–287.
- [44] K. Komnitsas, D. Zaharaki, A. Vlachou, G. Bartzas, M. Galetakis, Effect of synthesis parameters on the quality of construction and demolition wastes (CDW) geopolymers, *Adv. Powder Technol.* 26 (2015) 368–376.
- [45] D. Zaharaki, K. Komnitsas, Valorization of construction and demolition (C&D) and industrial wastes through alkali activation, *Constr. Build. Mater.* 121 (2016) 686–693.
- [46] A. Arulrajah, A. Mohammadinia, I. Phummiphon, S. Horpibulsuk, W. Samingthong, Stabilization of recycled demolition aggregates by geopolymers comprising calcium carbide residue, fly ash and slag precursors, *Constr. Build. Mater.* 114 (2016) 864–873.
- [47] L. Reig, M.V. Borrachero, J.M. Monzó, H. Savastano Jr., M.M. Tashima, J. Payá, Use of ceramic sanitaryware as an alternative for the development of new sustainable binders, *Key Eng. Mater.* 668 (2016) 172–180.
- [48] ASTM C1262-10, Standard Test Method for Evaluating the Freeze-Thaw Durability of Dry-Cast Segmental Retaining Wall Units and Related Concrete Units, ASTM, International, West Conshohocken, PA (2010) [www.astm.org](http://www.astm.org).
- [49] P. Duxson, J.L. Provis, G.C. Lukey, S.W. Mallicoat, W.M. Kriven, J.S.L. Van Deventer, Understanding the relationship between geopolymer composition, microstructure and mechanical properties, *Colloids Surf. A* 269 (2005) 47–58.
- [50] H.Y. Leong, D.E.L. Ong, J.G. Sanjayan, A. Nazari, The effect of different Na<sub>2</sub>O and K<sub>2</sub>O ratios of alkali activator on compressive strength of fly ash based-geopolymer, *Constr. Build. Mater.* 106 (2016) 500–511.
- [51] J.C. Swanepoel, C.A. Strydom, Utilization of fly ash in a geopolymeric material, *Appl. Geochem.* 17 (2002) 1143–1148.
- [52] J.G.S. Van Jaarsveld, J.S.J. Van Deventer, G.C. Lukey, The effect of composition and temperature on the properties of the fly ash- and kaolinite-based geopolymers, *Chem. Eng. J.* 89 (2002) 63–73.
- [53] W.K.W. Lee, J.S.J. Van Deventer, The effects of inorganic salt contamination on the strength and durability of geopolymers, *Colloids Surf. A* 212 (2002) 27–44.
- [54] H.M. Khater, H.A.A. Gawaad, Characterization of alkali activated geopolymer mortar doped with MWCNT, *Constr. Build. Mater.* 102 (2016) 329–337.
- [55] D. Rieger, T. Kovářik, J. Říha, R. Medlín, P. Novotný, P. Bělský, J. Kadlec, P. Holba, Effect of thermal treatment on reactivity and mechanical properties of alkali activated shale-slag binder, *Constr. Build. Mater.* 83 (2015) 26–33.
- [56] G. Socrates, Infrared and Raman Characteristic Group Frequencies, 3rd edition, John Wiley & Sons Ltd, Chichester, England, 2001.
- [57] D. Zaharaki, K. Komnitsas, V. Perdikatsis, Use of analytical techniques for identification of inorganic polymer gel composition, *J. Mater. Sci.* 45 (2010) 2715–2724.
- [58] S. Chuah, W.H. Duana, Z. Pan, E. Hunter, A.H. Korayem, X.L. Zhao, F. Collins, J.G. Sanjayan, The properties of fly ash based geopolymer mortars made with dune sand, *Mater. Des.* 92 (2016) 571–578.
- [59] W. Ren, J. Xu, E. Bai, Strength and ultrasonic characteristics of alkali-activated fly ash-slag geopolymer concrete after exposure to elevated temperatures, *J. Mater. Civil Eng.* 28 (2016), doi:[http://dx.doi.org/10.1061/\(ASCE\)MT.1943-5533.0001406](http://dx.doi.org/10.1061/(ASCE)MT.1943-5533.0001406).